American Journal of Mechanical Engineering, 2017, Vol. 5, No. 5, 205-210
Available online at http://pubs.sciepub.com/ajme/5/5/3

DOI:10.12691/ajme-5-5-3

Influence of Rotor Speed on Mixed Flow Turbine Performance

Ahmed Ketata*, Zied Driss

Laboratory of Electro-Mechanic Systems (LASEM), National School of Engineers of Sfax (ENIS), University of Sfax (US), B.P. 1173, Road Soukra km 3.5, 3038 Sfax, Tunisia
*Corresponding author: ketata.ahmed.enib@gmail.com

Abstract The radial turbine which is an important component of a turbocharger is used in automotive applications in order to enhance internal combustion engines performance. In the recent years, the radial turbine is commonly replaced instead of a mixed flow one. In fact, the mixed flow turbine yields to better aerodynamic performance at lower isentropic velocity ratio compared to the radial configuration. This present paper shows our numerical model under various steady conditions in purpose to understand the effect of the rotational speed on the turbine performance. Numerical simulations are conducted by solving the Reynolds averaged Navier Stokes equations using the CFX 17.0 package including a finite volume method for the discretization. To close these equations, the standard k-ε turbulence model is chosen. Our numerical model succeeds to predict the turbine performance and the swallowing capacity with an acceptable accuracy. Besides, the peak efficiency and the choking mass flow are computed for different operating conditions. Equally, the turbine reaction degree and power are given for each studied rotational speed. Then, the distribution of the total loss within the turbine is obtained numerically at different operating conditions.

Keywords: *CFD, turbulence, mixed-flow turbine, performance, mass flow, efficiency, loss*

Cite This Article: Ahmed Ketata, and Zied Driss, "Influence of Rotor Speed on Mixed Flow Turbine Performance." *American Journal of Mechanical Engineering*, vol. 5, no. 5 (2017): 205-210. doi: 10.12691/ajme-5-5-3.

1. Introduction

To reduce the dioxide carbon emissions from automotive internal combustion engines, car manufacturers use small engines by means of the downsizing technics. For such engines, a boosting system such a turbocharger becomes required to reward the engine output power loss. A turbocharger which plays a vital role in the success of downsized engines consists mainly of a radial turbine and a centrifugal compressor. The turbocharger turbine recovers the engine exhaust gas energy and converts it into a rotational energy on the turbocharger compressor shaft. Most of the recent research works tend to enhance the turbocharger turbine aerodynamic performance and to reduce the occurring losses by studying the effect of its geometrical parameters and the operating conditions. In the last decades, the use of mixed flow turbine instead of a radial one became more popular in automotive applications. In fact, the mixed flow turbine allows working at the same level of the efficiency compared to the radial turbine but at lower isentropic velocity ratio. Equally, mechanical stresses, as well as the fatigue failure risk of the turbine bearing, are reduced significantly when the mixed flow turbine is used. Among the earliest investigations of a mixed flow rotor is the work done by Hamerick et al. [1]. They analyzed the compressible flow within an arbitrary centrifugal mixed flow impeller in the meridional plane assuming that the flow is non-viscous. Then, Wallace [2] investigated a small mixed flow turbine for automotive applications. He indicated the advantage of the use of a mixed flow turbine instead of a radial one. Waston and Jonata [3] made a comparison between a mixed flow turbine and a radial turbine. They showed that the mixed flow turbine works efficiently at a lower velocity ratios compared to the radial configuration. Abidat [4] designed and tested two highly loaded mixed flow turbines. He proved that both mixed flow rotors achieve their peak efficiency at lower optimum velocity ratios compared to the radial turbine. In various anterior works, A one-dimensional code including a mean line model has been used to predict the turbine overall performance [5,6]. Romagnoli and Martinez-Botas [7] developed a meanline model including several loss models to predict the nozzleless and nozzled mixed flow turbines performances under different rotational speeds. Their model showed a good agreement with the test data. The mean line model stills useful for industrial applications. However, it presents some limitations compared to the computational fluid dynamics (CFD) simulations. Among the earliest CFD simulation is of Lymberopoulos et al. [8] in which a quasi-three-dimensional solution based on the Euler equation was developed. Chen el al. [9] developed three-dimensional computations for the prediction of the performance of different mixed flow turbine under several rotational speeds. They specified that the blade number has a considerable impact on the turbine performance. Furthermore, their results showed that the turbine performance is significantly sensitive to the rotational

speed. Hamel et al. [10] reported the capability of the k-ε turbulence model and the frozen rotor approach to give accurate results of the turbine performance. Karamanis et al. [11] investigated on a mixed flow turbine at five different rotational speeds under steady conditions. Their results indicated that the total to static efficiency of the turbine increases with the rotational speed until an operating limit and then, it becomes constant. Padzillah et al. [12] conducted a three-dimensional numerical steady simulation to predict a mixed flow turbine performance for a broad range of the rotational speed. They affirmed the ability of CFD as an advanced tool to calculate accurately the aerodynamic performance of the turbine and different flow parameters. They reported that the rotational speed of the turbine rotor presents a significant impact on its efficiency.

As a literature review, it is evident that most anterior works for turbocharger turbines are based on the turbine performance maps prediction by solving a one-dimensional code almost integrated with a mean line model. In view of the incapability of the average line model for giving a thorough analysis, the computational fluid dynamics simulations become popular and allow to understand with a detailed manner the flow behavior into such turbine in purpose to improve its efficiency. This paper presents our optimized CFD model in order to predict the steady-state performance of a vanned mixed flow turbine under different operating conditions. Firstly, the turbine geometry model and the meshing are developed. Then, the turbine performance maps are computed by solving the RANS equations. A good agreement is found between our numerical results and the experiments. Furthermore, the degree of reaction and the available shaft power of the turbine are computed for each operating conditions. Then, the distribution of the total loss within the full turbine stage is obtained numerically as a function of the incidence angle.

2. Turbine Geometry

The mixed flow turbine becomes popular in automotive applications. For such turbine, the flow velocity at the rotor inlet has axial and radial components. Its design permits to obtain a non-zero inlet blade angle with maintaining of radial fiber elements rule. It allows working efficiently at lower velocity ratio and then, to improve the pressure boost at the engine intake. In this work, we are interested in a mixed flow turbine which consists of a rotor, a vane, and a volute. The impeller blade shape is made with Polynomial Bezier curves giving different control points. More detailed geometrical parameters of the present rotor are available in the litterature [4,7]. Figure 1 shows the developed three-dimensional model of the full mixed flow turbine stage.

The inflow radius of the turbine vane is about 70 mm. However, the volute is a commercial vaneless one. Rajoo [13] transformed it to acquire a nozzle ring and then, the volute can be nozzled or nozzleless. In this application, we are interested in the nozzleless configuration of the volute. Its centroid throat radius and its throat area are respectively about 100 mm and 3300 mm^2. The tongue position is fixed to be 50°.

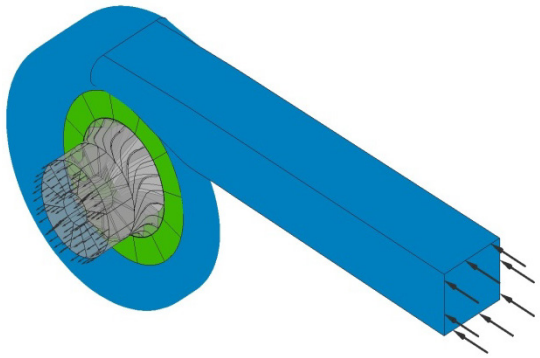

Figure 1. Computational domain

3. Numerical Model

Numerical solutions are obtained by solving implicitly Reynolds averaged Navier-Stokes equations of mass, momentum, and energy conservation for a compressible flow using the commercial Ansys CFX 17.0 package. Equally, a finite volume method is utilized for discretization. To close the terms issues from the Reynolds decomposition, the standard k-ε turbulence model is chosen. The turbulence model showed a good ability to capture the flow in several anterior aerodynamic works [14,15]. The rotating domain is modeled by a frozen rotor approach. This method is used previously in anterior works and allows a good accuracy of the numerical results [16]. To model the same conditions at the test rig, a total pressure and a total temperature are defined at the turbine inflow boundary for each tested rotational speed. However, an average static pressure instead of a static pressure is determined at the turbine exit to avoid the creation of the reverse flow during the computing process. Table 1 presents different total pressures and total temperatures set at the turbine inflow at each rotor speed. Furthermore, zero values are affected by all parameters as initial conditions of the computational domain. The accuracy of the numerical results depends significantly on the mesh quality and size. Our computational domain of the full turbine stage is meshed with tetrahedral elements. The volute tongue, the rotating interface, and the rotor are refined more than other regions. Furthermore, an inflation of ten prism layers is applied to the wall near zones by setting the first cell high. This inflation is used to guarantee that the non-dimensional wall distance is in the range required by the turbulence model. The generated meshing consists of 329619 cells and 106070 nodes. Figure 2 presents a three-dimensional view of the obtained unstructured mesh of the turbine volute and impeller.

Table 1 Boundary conditions.

N (rpm)	P_{01} (Pa)	T_{01} (K)
59783.4	213996	343
52628.6	190000	341
47502.8	170000	339
41414.6	148000	337
35361.4	135000	335
30547.6	119000	333

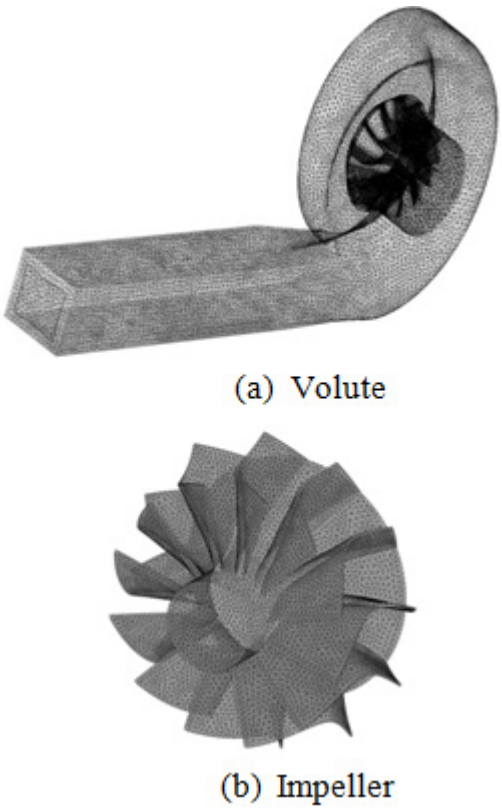

Figure 2. 3D view of the meshing

4. Numerical Validation

To validate our numerical model, a comparison of the computed results to test data is performed. In fact, the distribution of the total to static isentropic efficiency is calculated as a function of the mass flow parameter. Figure 3 presents the superposition of the distribution of the computed total to static isentropic efficiency and the experimental data collected by Romagnoli [7] for a rotationnel speed of 59783.4 rpm. A good agreement has been observed between the experimental and numerical results. However, a small gap between the computed and measured turbine performance is noted, but it stills in an acceptable range. This fact confirms the validation of our numerical model.

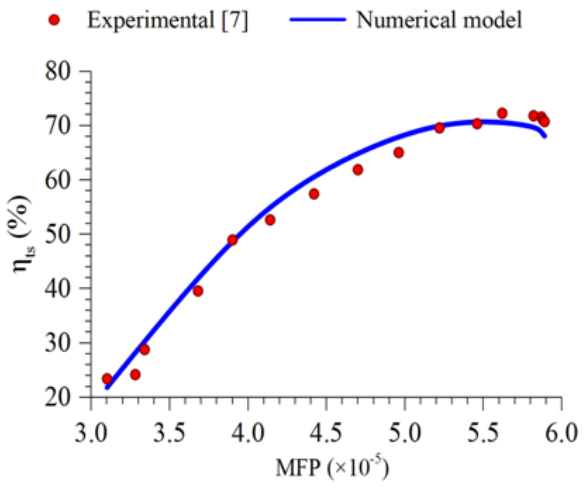

Figure 3. Comparison with test data

5. Results and Discussion

5.1. Efficiency

Figure 4 presents the distribution of the total to static isentropic efficiency as a function of the isentropic velocity ratio for different rotational speeds. From these results, it has been observed that the total to static isentropic efficiency gets an upward trend when the velocity ratio decreases until it attains its maximum value. From this point, it returns to drop slightly. It can be seen that the peak efficiency occurs at a velocity ratio less than 0.7 which presents typically the point of the peak efficiency for a radial inflow turbine. Then, the mixed flow turbine works efficiently at lower velocity ratios compared to the radial configuration. From 41414.6 rpm to 59783.4 rpm, the efficiency remains at the same level for a velocity ratio higher than 0.85. The same observation is obtained from 30547.6 rpm to 35367.4 rpm for a velocity ratio greater than 0.6. However, the isentropic efficiency becomes significantly more sensitive to the rotational speed for lower velocity ratios. At these conditions, the efficiency increases with the drop in the rotational speed until it achieves a higher value from it returns to decrease.

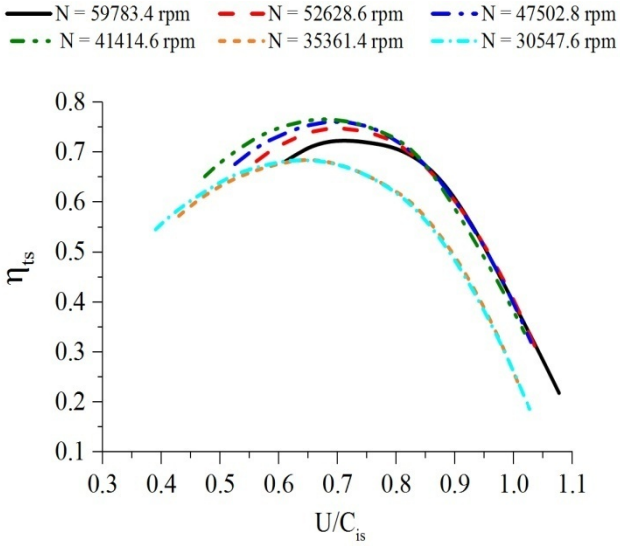

Figure 4. Efficiency map

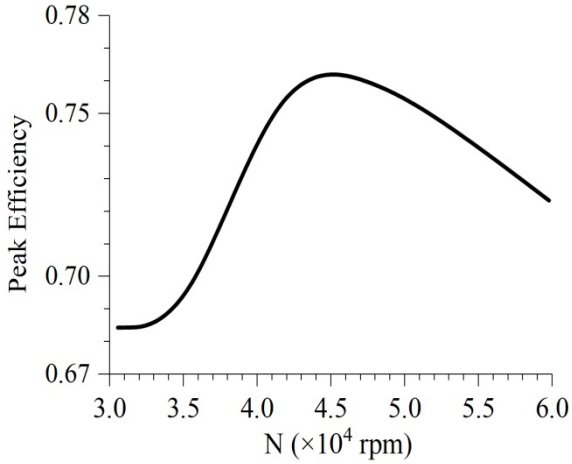

Figure 5. Distribution of the peak efficiency

In order to evaluate the effect of the operating conditions on the turbine stage performance, the peak efficiency is plotted as a function of the rotational speed as shown in Figure 5. From these results, it is worth noting that the peak efficiency depends greatly on the rotational speed.

From the lowest rotor speed to 3300 rpm, the peak efficiency remains at the same level about 0.685. From 3300 rpm to 4500 rpm, the peak efficiecny increases with a strong slope. At 45000 rpm, the peak efficiency reaches its maximum value of 0.761. At this rotational speed, the turbine seems to recover the maximum amount of the available exhaust gas energy. From this optimum point, the peak efficiency decreases slightly with the rise of the rotor speed.

5.2. Mass Flow

Figure 6 presents the distribution of the reduced mass flow as a function of the expansion ratio for different operating conditions. Referring to Figure 6, it has been noted that the mass flow parameter increases, with a nonlinear trend, with the surge of the pressure ratio for different rotational speeds. At higher pressure ratios, the mass flow parameter still nearly in the same level. At these conditions, the mass flow rate becomes approximately insensitive to the change of the pressure ratio. This limitation of the mass flow rate is referred to the choked flow which is a characteristic of the sonic blockage. At this zone of the turbine map, an aerodynamic loss which is due to the flow blockage occurs. Furthermore, any choking condition is observed for both 30547.6 rpm and 35361.4 rpm of the rotational speed. The maximum recorded value of the choking mass flow parameter is found to be 0.614 at 41414.6 rpm of the turbine speed. When the pressure ratio is fixed at a defined value, it can be clearly detected that the mass flow rate is greatly sensitive to the turbine speed. Indeed, the mass flow rate as well as the choking mass flow rate decreases significantly with the surge of the rotational speed.

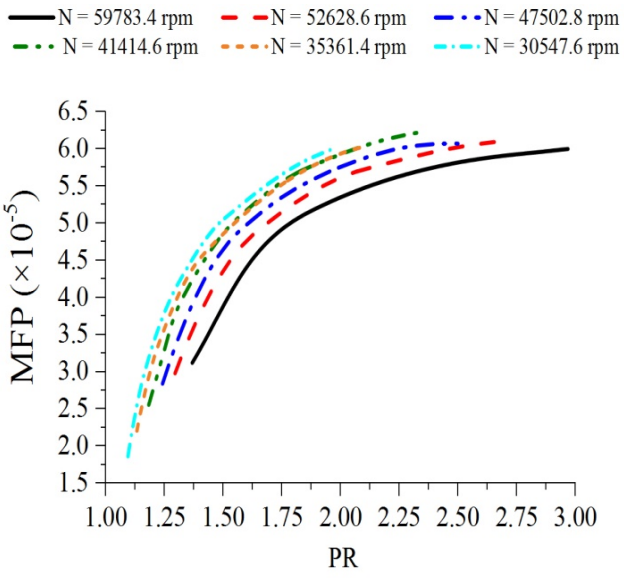

Figure 6. Mass flow map

Figure 7 shows the distribution of the choking mass flow parameter as a function of the rotational speed for different operating conditions. From these results, it is evident that the choking mass flow rate depends considerably on the turbine speeds. From 30546.7 rpm, the choking mass flow parameter increases rapidly until it achieves its highest point about 6.23 105 which is recorded at about 42000 rpm. After, the choking mass flow parameter decreases with the rise of the rotational speed excluding the zone between 47000 rpm and 52000 rpm which shows a slight increase of the choking mass flow parameter.

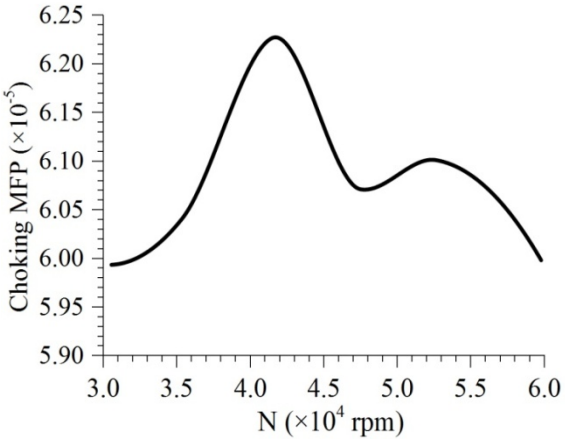

Figure 7. Distribution of the mass flow parameter at the choking point

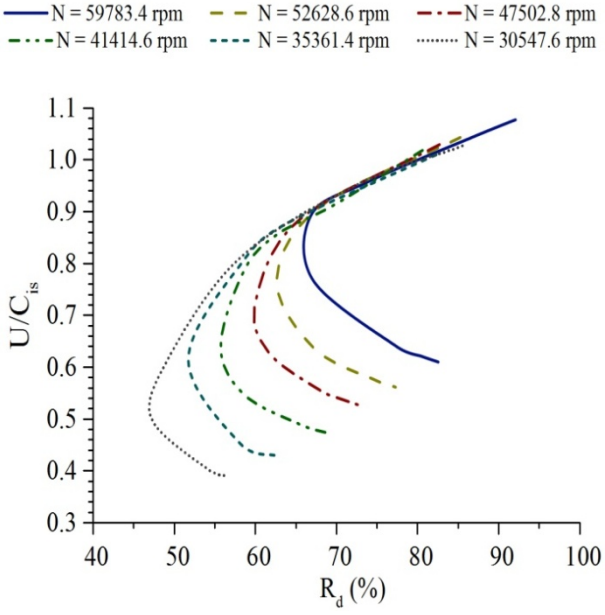

Figure 8. Degree of reaction against velocity ratio

5.3. Reaction Degree

Figure 8 presents the distribution of the turbine degree of reaction as a function of the velocity ratio at different rotational speeds. From these results, it has been observed that the value of the degree of reaction varies significantly with the change of the velocity ratio and then, with the pressure ratio for different speeds of the rotor. In fact, at a fixed value of the speed, the degree of reaction decreases

gradually with the rise of the velocity ratio from its lowest value. Once a minimum value is reached, the degree of reaction gets an upward trend with a sharp slope. Furthermore, it has been observed that the reaction degree presents approximately the same value for different speeds of the rotor at a fixed value of the velocity ratio higher than 0.9. However, the degree of reaction is found to be exceedingly sensitive to the rotor speed for velocity ratios less than 0.9. In this case, the rise of the rotational speed yields to the growth of the reaction degree. Thus, the contribution of the mixed flow rotor to the enthalpy drop within the full turbine stage is more important at higher rotational speeds. For 30547.6 rpm, there is a small zone of the distribution of the degree of reaction in which it is found to be less than 50%. At this zone, the contribution of the stator to the total work within the turbine stage is more significant compared to that of the rotor.

5.4. Output Power

Figure 9 shows the available power of the turbine against the isentropic velocity ratio for different operating conditions. From these results, it can be observed that the turbine generated power is considerably sensitive to the change of the isentropic velocity ratio. In fact, the produced power on the turbine shaft decreases significantly when the velocity ratio gets a downward trend. Thus, higher power values are reached at higher pressure ratios. When the rotor blades become highly loaded, the turbine shaft torque, as well as the available power, takes greater values. At a fixed value of the turbine expansion ratio, the available power in the turbine shaft increases considerably with the rise of the rotor speed, especially at higher expansion ratios. For example, the available power in the turbine shaft is found to be about 33.3 kW at the optimum isentropic velocity ratio for 59783.4 rpm of the rotor speed. However, it decreases sharply to be about 3.6 kW at the optimum isentropic velocity ratio for 30547.6 rpm. As a result, more the turbine expansion ratio and its shaft rotational speed are greater, more the available power in the turbine shaft is important.

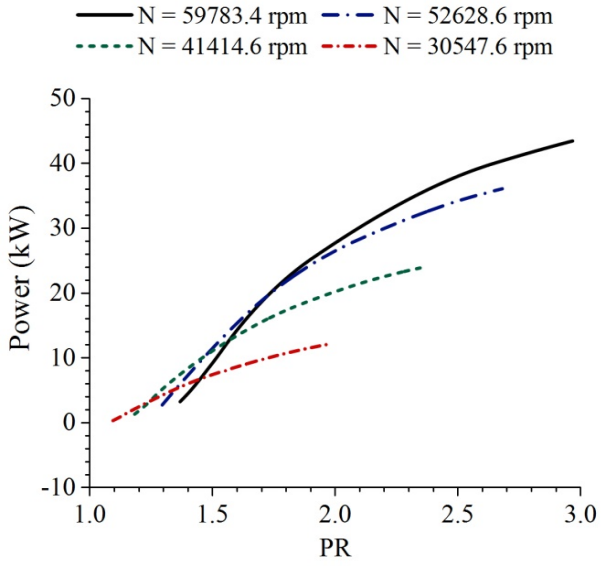

Figure 9. Available power vs. Pressure ratio

5.5. Total Loss

Figure 10 presents the distribution of the overall aerodynamic loss within the turbine as a function of the incidence angle at different operating conditions. From these results, it is evident that the total generated loss is significantly sensitive to the variation of the incidence angle. In fact, from lowest incidence angles, the total loss decreases with a sharp slope when the incidence angle increases until it takes a minimum value. From this last point, the total loss turns to grow slightly with the increase of the incidence angle. Thus, it can be concluded that the minimum values of the total loss occur at negative incidence angles for different speeds of the rotor. For example, the minimum total loss, which is about 25.4 %, is recorded at about -53° of the incidence angle for 52628.6 rpm of the rotational speed. For 41414.6 rpm, the minimum overall loss about 23.8 % is recorded at -31.5° of the incidence angle. Thus, the minimum total loss is obtained at slightly negative incidence angles for lower rotational speeds. At higher rotor speeds, the total loss takes its minimum values at higher absolute values of the incidence angle. At a fixed value of the incidence angle, it has been observed that the total loss increases practically with the rise of the rotational speed for absolute values of the incidence angle higher than 70°. As a result, the growth of the rotational speed yields to higher values of the total loss within the turbine stage in this range of the incidence angle. However, it has been observed that when the incidence angles are lower than -70°, the total loss becomes insensitive to the rotational speed of the turbine.

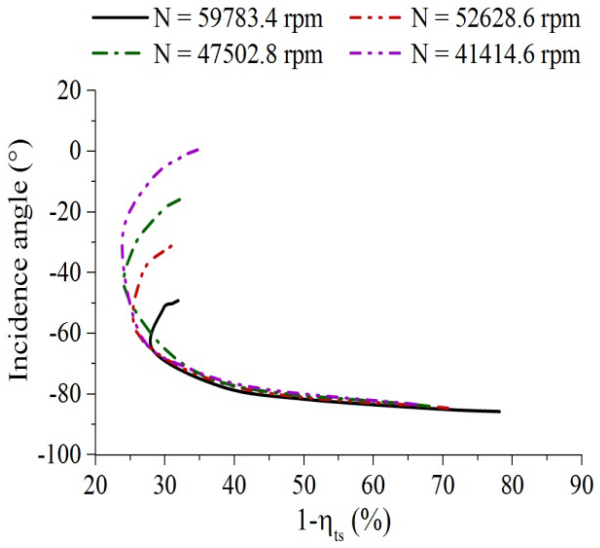

Figure 10. Total loss vs. Incidence angle

6. Conclusion

Computational fluid dynamics simulations are successfully conducted by solving the Reynolds averaged Navier Stokes equations. A reasonable agreement is found between the numerical results and the test data confirming the validity of our numerical model. Our numerical results show that the mass flow rate and the efficiencies of the turbine are significantly sensitive to the operating conditions. At the choking point, the mass flow becomes

insensitive to the pressure ratio. However, the peak efficiency occurs at an optimum velocity ratio less than 0.7 which is typically the optimum point for a radial turbine. Furthermore, the peak efficiency and the choking mass flow depend greatly on the rotational speed. The same observation is obtained for the turbine reaction degree. Equally, higher power values are reached at higher rotational speeds and expansion ratios. The total loss within the full turbine stage depends considerably on the rotor inlet incidence angle and also to the rotational speed. However, for incidences angles lower than -70°, the total loss becomes approximately insensitive to the speed of the turbine. Additionally, minimum values of the total loss are practically recorded at negative incidence angles at a full range of the rotational speed.

Nomenclature

MFP	mass flow parameter, $kg.s^{-1}.\sqrt{K}.Pa^{-1}$
N	rotational speed, rpm
PR	Pressure ratio, dimensionless
R_d	degree of reaction, dimensionless
η	isentropic efficiency, dimensionless.

References

[1] J. T. Hamerick, A. Ginsburg, W. M. Osborn. Method of analysis for compressible flow through mixed-flow centrifugal impellers of arbitrary design, NASA Report No. TN 2165. 1950.

[2] Wallace, F. J., "A Systematic Approach to the Design of Radial Inflow and Mixed Flow Turbines," NACA Report No. CP 1180. 1971.

[3] N. Watson, M.S. Janota, Turbocharging the internal combustion engine. Macmillan, London, 1982.

[4] M. Abidat, Design and testing of a highly loaded mixed flow turbine. PhD thesis, Imperial College, London, 1991.

[5] S. M. Futral, C. A. Wasserbauer, Off design performance prediction with experimental verification for a radial-inflow turbine, NASA TND-2621 (1965).

[6] A. J. Glassmann, C. A. Wasserbauer, Fortran program for predicting off-design performance of radial inflow turbines, NASA TN-D-8063 (1975).

[7] A. Romagnoli, R. F. Martinez-Botas, Performance prediction of a nozzled and nozzleless mixed-flow turbine in steady conditions, International Journal of Mechanical Science 53 (2011). 557-574.

[8] N. Lymberopoulos, N. C. Baines, N. Watson, Flow in single and twin entry radial turbine volutes, ASME Gas Turbine and Aeroengine Congress (1988). paper 88-GT-59.

[9] H. Chen, M. Abidat, N.C. Baines, M.R. Firth, The effect of blade loading in radial and mixed flow turbines, ASME (1992) Paper No 92-GT-92.

[10] M. Hamel, M. Abidat, S.A. Litim, Investigation of the mixed flow turbine performance under inlet pulsating flow conditions, C. R. Mecanique 340 (2012). 165-176.

[11] N. Karamanis, R.F. Martinez-Botas, C.C. Su, Mixed flow turbines: Inlet and exit flow under steady and pulsating conditions, J Turbomach 123 (2001). 359-371

[12] M.H. Padzillah, S. Rajoo, M. Yang, R.F. Martinez-Botas, Influence of pulsating flow frequencies towards the flow angle distributions of an automotive turbocharger mixed-flow turbine, Energy Conversion and Management 98 (2015). 449-462.

[13] S. Rajoo, Steady and Pulsating Performance of a Variable Geometry Mixed Flow Turbochager Turbine, PhD thesis, Imperial College, London, 2007.

[14] Z. Driss, O. Mlayeh, S. Driss, D. Driss, M. Maaloul, M. S. Abid, Study of the incidence angle effect on the aerodynamic structure characteristics of an incurved Savonius wind rotor placed in a wind tunnel, Energy 894 (2016). 908-113.

[15] Z. Driss, O. Mlayeh, D. Driss, M. Maaloul, M. S. Abid, Numerical simulation and experimental validation of the turbulent flow around a small incurved Savonius wind rotor, Energy 74 (2014). 506-17.

[16] J. W. Lam, Q. Roberts, G. McDonnel, Flow modelling of a turbocharger turbine under pulsating flow, Preceedings of IMechE International Conference on Turbochargers.